On the Vertical Structure of Modeled and Observed Deep Convective Storms: Insights for Precipitation Retrieval and Microphysical Parameterization

JAMIE L. SMEDSMO, EFI FOUFOULA-GEORGIOU, AND VENUGOPAL VURUPUTUR

Saint Anthony Falls Laboratory, Department of Civil Engineering, University of Minnesota, Minneapolis, Minnesota

FANYOU KONG

Center for Analysis and Prediction of Storms, The University of Oklahoma, Norman, Oklahoma

KELVIN DROEGEMEIER

Center for Analysis and Prediction of Storms, and School of Meteorology, The University of Oklahoma, Norman, Oklahoma

(Manuscript received 30 September 2004, in final form 2 June 2005)

ABSTRACT

An understanding of the vertical structure of clouds is important for remote sensing of precipitation from space and for the parameterization of cloud microphysics in numerical weather prediction (NWP) models. The representation of cloud hydrometeor profiles in high-resolution NWP models has direct applications in inversion-type precipitation retrieval algorithms [e.g., the Goddard profiling (GPROF) algorithm used for retrieval of precipitation from passive microwave sensors] and in quantitative precipitation forecasting. This study seeks to understand how the vertical structure of hydrometeors (liquid and frozen water droplets in a cloud) produced by high-resolution NWP models with explicit microphysics, henceforth referred to as cloud-resolving models (CRMs), compares to observations. Although direct observations of 3D hydrometeor fields are not available, comparisons of modeled and observed radar echoes can provide some insight into the vertical structure of hydrometeors and, in turn, into the ability of CRMs to produce precipitation structures that are consistent with observations. Significant differences are revealed between the vertical structure of observed and modeled clouds of a severe midlatitude storm over Texas for which the surface precipitation is reasonably well captured. Possible reasons for this discrepancy are presented, and the need for future research is highlighted.

1. Motivation

a. Passive microwave rainfall retrieval

The Tropical Rainfall Measuring Mission (TRMM) satellite was launched in 1997, carrying five instruments, two of which specifically were designed for the measurement of precipitation: the TRMM precipitation radar (PR) and the TRMM Microwave Imager (TMI) (Kummerow et al. 2000). The TMI has four dual-polarized spectral bands and one spectral band with only vertical polarization. Although several algorithms utilize TMI measurements for estimating precipitation (ostensibly rainfall and referred to as such hereinafter) at various space and time scales, the present discussion focuses on the Goddard profiling (GPROF) algorithm, which is used to estimate orbit-based hydrometeor profiles and surface precipitation rate for every pixel viewed by TMI (see Kummerow et al. 2001).

Retrievals of surface instantaneous precipitation from the TMI GPROF algorithm depend heavily upon assumptions about the microphysics and structure of rain-producing clouds (Kummerow et al. 2001; Adler et al. 2003). Because the microwave imager is sensitive to the entire vertical structure of the hydrometeor field within the cloud, TMI estimates of precipitation are thus indirectly derived from the vertical hydrometeor profile. A database consisting of cloud hydrometeor and thermodynamic profiles is constructed using cloud-resolving model (CRM) simulations, and then associ-

Corresponding author address: Dr. Efi Foufoula-Georgiou, Saint Anthony Falls Laboratory, Dept. of Civil Engineering, University of Minnesota, Mississippi River at Third Ave. SE, Minneapolis, MN 55414.
E-mail: efi@umn.edu

ated brightness temperatures are computed with radiative transfer calculations through the simulated clouds. Hydrometeor retrieval is achieved by a conditional inversion algorithm that matches brightness temperatures observed at the top of the cloud to a cloud profile with the same brightness temperatures in the preexisting database. The inversion algorithm utilizes both emission and scattering signals derived from the nine TMI bands. Over land, high emissivity, which also varies depending upon surface characteristics, creates high and unpredictable surface emissions that mix with emissions from clouds (Kummerow et al. 2001), making emission signals unusable for precipitation estimation.

Although the TRMM has led to great advances in the estimation of precipitation in areas where routine observations are not available, significant biases and uncertainties remain. Biases between different TRMM algorithms and between TRMM algorithms and ground-based measurements probably are caused by problems with physical assumptions upon which the algorithms are based. These biases vary geographically, seasonally, and annually (Kummerow et al. 2001; Adler et al. 2003). Adler et al. (2003) examined TRMM precipitation products from five different algorithms, comparing them with precipitation estimates from the Global Precipitation Climatology Project and to rain gauge measurements and performing global intercomparisons between the TRMM products. Because the GPROF and PR algorithms depend upon cloud structure and microphysics in different ways, comparing the two products may give an indication of where the assumptions break down. While several issues may contribute toward the observed regional biases, including variations in horizontal inhomogeneity that cause the "beamfilling error" (e.g., Wilheit 1986) and low-level humidity errors (McCollum et al. 2000), we focus here on the effects of variations in cloud vertical structure on passive microwave remote sensing of precipitation.

The vertical structure of precipitation affects passive microwave rainfall retrieval because the emission bands of the microwave sensor are sensitive to the column-integrated liquid water content and not just to precipitation on the ground (e.g., Wilheit et al. 1977). To estimate the surface rain rate for a TMI pixel, the vertical distribution of hydrometeors must first be determined (Kummerow et al. 2001). The first step in this process is to determine the freezing level and, therefore, rain layer thickness. This first part of the algorithm presents problems when only warm-rain processes occur (e.g., Short and Nakamura 2000). The second step is to distribute the hydrometeors vertically from the freezing level to the surface. Because this step is done using an inversion algorithm based upon the cloud database, it will be inaccurate if the vertical distribution of water in a storm is not represented accurately or at all within the database or if a problem exists with the radiative transfer calculations.

A second aspect of the vertical profile has been highlighted in several recent field studies in tropical regions and is a major concern over land. It has been shown that, in a single location, the vertical extent and strength of precipitating convective storms can vary on time scales of days to weeks (Rutledge et al. 1992; Williams et al. 1992; Cifelli and Rutledge 1998; Cifelli et al. 2002; da Silva Dias et al. 2002; Halverson et al. 2002). In clouds with deeper vertical extent, more ice may be present for the same amount of precipitation on the ground relative to a shallower cloud. Berg et al. (2002) identified the biases in rainfall retrieval that result from differences in the vertical structure of storms between the eastern and western Pacific Ocean when remote sensing algorithms ignore variability in the relationship between cloud ice profiles and surface rain rate. The lack of emission bands over land means that precipitation must be derived from ice scattering. Although these types of algorithms have met with some success, they generally are less accurate than emission algorithms or combined emission–scattering algorithms because ice processes are not directly related to precipitation on the ground (Kummerow and Giglio 1994; Kummerow et al. 2001). Fu and Liu (2001) showed that, given the same rain rate on the ground, variations in precipitation vertical profiles as observed by TRMM PR correspond to large differences in brightness temperatures observed by TMI in both the emission and scattering frequencies. It may be important to condition the rainfall on the vertical structure of ice in the storm, especially over land.

b. Hydrometeor profiles in quantitative precipitation forecasting (QPF)

Microphysical processes may be parameterized in CRMs using models of varying complexity. Because of limited computational resources, microphysical models often are rudimentary. For example, a common bulk microphysics parameterization scheme created by Lin et al. (1983) and used in several CRMs (Tao and Simpson 1993; Xue et al. 2001) is known to have limited success in accurately representing cloud processes (Ferrier et al. 1995) but has generally been viewed as sufficient to simulate the morphology of thunderstorms reasonably well. Improvements to parameterizations also are hampered by paucity of in situ observations. Although microphysical probes provide information about hydrometeors present along the flight path of a research aircraft, remote sensing techniques are not yet

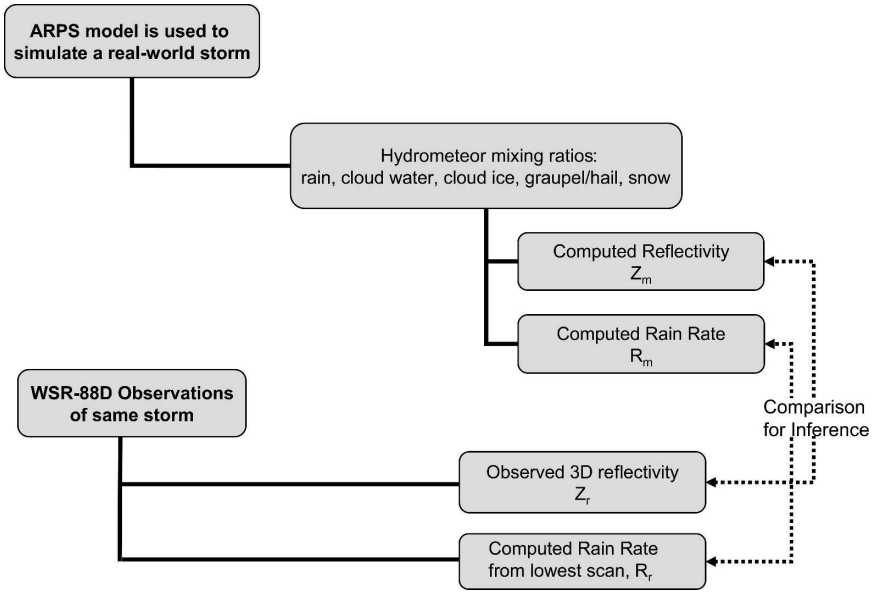

FIG. 1. Diagram of the numerical experiment designed to address the research objectives.

able to provide accurate quantitative 3D fields of hydrometeors. In the report of the Eighth Prospectus Development Team commissioned by the U.S. Weather Research Program on Quantitative Precipitation Forecasting, Fritsch et al. (1998) state that "A key issue related to microphysics research is that very little work has been done to verify cloud hydrometeor predictions (or simulations) with observations." While they acknowledge the difficulty in comparing radar-derivable parameters with hydrometeor predictions, they suggest that some comparison of predicted 3D hydrometeor fields with observations is a key step in verifying the models used in QPF. In a more recent report to the science steering committee of the U.S. Weather Research Program on Research and Development to Improve Quantitative Precipitation Forecasts in the Warm Season (Fritsch and Carbone 2004), it was again emphasized that a better understanding of microphysical properties and processes is a key to improving QPF, especially during the summer when deep, moist convection is a dominant precipitation formation process.

The goal of this research is to investigate the statistical structure of hydrometeor fields predicted by CRMs and to provide an assessment of how well CRMs can reproduce the vertical structure of observed storms. The Advanced Regional Prediction System (ARPS), with explicit microphysics and 1-km grid spacing, was used to simulate 3D precipitating clouds for a deep convective midlatitude storm over Fort Worth, Texas, for which vertical reflectivity observations were also available. Section 2 provides details of the simulation and the available observations. Section 3 compares the modeled and observed storms in terms of the statistical structure of surface rain, and section 4 compares them in terms of the statistical structure of reflectivity profiles. Conclusions, interpretations, and issues for further research are discussed in section 5.

2. Description of modeled storm and radar observations

a. The ARPS model

A numerical experiment, schematically depicted in Fig. 1, is used in this study to compare the vertical structure of modeled and observed deep convective storms. An observed storm was modeled by ARPS, a three-dimensional nonhydrostatic mesoscale modeling system developed at the Center for Analysis and Prediction of Storms (CAPS) at The University of Oklahoma. The ARPS is a flexible system for use in basic and applied research as well as in real-time prediction of weather events. The ARPS provides modules for start-to-finish modeling of real-world or idealized cases; it includes 1) a data ingest, quality control, and objective analysis package and a data assimilation system, 2) a forward prediction component, and 3) a postprocessing, diagnostic, and verification package (Xue et al. 2001). A complete description is given in the ARPS, version 4.0, user's guide (Xue et al. 1995), with more recent updates described in (Xue et al. 2000, 2001, 2003).

One of the original goals of ARPS was the inclusion

of a sophisticated data assimilation scheme that could handle data from the newly deployed Weather Surveillance Radar-1988 Doppler (WSR-88D) network as well as several other data sources relevant to mesoscale NWP. The ARPS Data Assimilation System (ADAS; Brewster 1996, 2002, 2003) can incorporate data from many sources, including input from a large-scale model, WSR-88D radars, satellites, rawinsondes, and surface observations. It also includes a cloud analysis component to create three-dimensional fields of hydrometeors and a 4D variational velocity adjustment and thermodynamic retrieval component to provide input for the ARPS forecast components (Xue et al. 1995, 2003). In this study, WSR-88D level-III reflectivity and radial velocity data were assimilated in the ARPS forecast.

The ARPS forward prediction module operates on a finite-difference approximation of the fully compressible Navier–Stokes equations, as well as thermodynamic and microphysical processes, using as few physical approximations as possible. The system of equations is solved on a curvilinear coordinate system that allows for horizontal and vertical stretching and ensures that the lower boundary conforms to the terrain. Three subgrid-scale closure options are available for the turbulent mixing terms (Xue et al. 2000); the 1.5-order turbulent kinetic energy closure scheme is used in the model runs discussed in this paper.

Surface processes are characterized using the land surface state to calculate the surface energy and moisture budget. The thermal energy budget includes net radiation, sensible heat fluxes, and heat flux into the ground. The surface moisture budget includes precipitation and dew formation, direct evaporation from the ground and vegetation canopy, evapotranspiration, runoff, and surface turbulent moisture flux. Lower boundary conditions for heat and momentum flux are provided with parameterizations of the drag coefficients (Xue et al. 2001).

Precipitation processes are divided into grid-scale and parameterized convective precipitation. Grid-scale precipitation is explicitly determined by microphysical processes, but subgrid-scale convective precipitation processes must be parameterized using various simplified physical models. Two microphysical schemes are available, the Kessler warm-rain scheme (Kessler 1969) and the Lin et al. (1983) five-category water and ice scheme (including cloud water, rain, cloud ice, hail/graupel, and snow) as implemented by Tao and Simpson (1993). The scheme assumes an exponential size distribution for rain, snow, and hail/graupel, and cloud water and cloud ice have a constant size (Xue et al. 2001). Processes for conversion among hydrometeor species and condensation and evaporation are parameterized. The ARPS includes two different cumulus parameterization schemes, the Kuo scheme (Kuo 1965, 1974) and the Kain–Fritsch scheme (Kain and Fritsch 1993); the latter is used in this study.

b. The Fort Worth storm

1) ARPS FORECAST

The ARPS was used to simulate a tornadic thunderstorm that moved through Fort Worth on 28 and 29 March 2000. In addition to causing extensive wind damage to a major metropolitan area, the storm produced torrential rain and softball-sized hail. This case study was run at CAPS with other research objectives in mind. Researchers wanted to test the ability to initialize a model with preexisting thunderstorms and predict their development and also wanted to assess the effect of a data assimilation cycle using sophisticated WSR-88D data analysis on the ability of the ARPS model to predict a real-life weather event. Observed meteorological conditions and details of the model setup for the Fort Worth storm are given in Xue et al. (2003). The case was studied extensively, both with single forecasts and ensembles, with the conclusion that it reproduced the timing, location, and key characteristics of a convective storm with good accuracy (Kong et al. 2004; Levit et al. 2004). This case was selected for this study because, from a meteorological standpoint, the model did a good job of reproducing the observed events, at least qualitatively. We will use this case to assess the ability of a mesoscale model to produce hydrometeor profiles that are physically consistent with observed radar echoes. This assessment is done indirectly by comparing the spatial and vertical structure of observed 3D reflectivity fields with reflectivity fields predicted from modeled clouds (see Fig. 1).

The ARPS model was applied using one-way grid nesting with three nests, implying no feedback among them apart from boundary-condition information. The National Centers for Environmental Prediction (NCEP) Eta Model analysis at 1800 UTC 28 March with no radar data assimilation was used as initial conditions for a model run with 9-km horizontal grid spacing. The NCEP Eta Model forecast starting at 1800 UTC 28 March was used to provide lateral boundary conditions at 3-h intervals. The 9-km forecast was run for 12 h. The 3-km nested grid was initiated at 2200 UTC using initial and lateral boundary conditions provided by the 9-km grid. The 3-km grid covered a domain of 450×300 km^2 and employed full model physics but no cumulus parameterization. The 3-km grid was initialized with four data assimilation cycles at 15-min intervals, using WSR-88D level-III reflectivity and

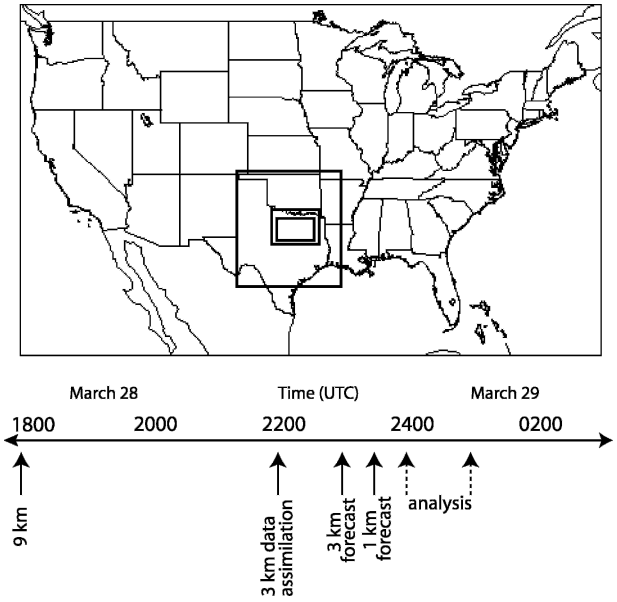

FIG. 2. Diagram depicting the time and space domain for the Fort Worth model. (top) The map shows the nested domains of the runs with 9-, 3-, and 1-km grid spacing. (bottom) The time line shows the start times for each of the model runs with solid arrows and shows the analyzed time domain with broken arrows.

radial velocity data from several radars, along with National Weather Service surface observations (Xue et al. 2003). Hence, the true forecast started at 2300 UTC. Because the model was initialized using a data assimilation cycle with storms already in progress, model spinup time was reduced. A fine grid having a horizontal grid spacing of 1 km was initialized from the 3-km model at 2330 UTC. The 1-km grid covered a domain of 350×210 km^2 and also employed full model physics except for cumulus parameterizations. A schematic of the model domains is shown in Fig. 2.

All simulations were run using a terrain-following, stretched vertical grid with grid spacing increasing from 20 m near the surface to 760 m near the top (which exceeded 20 km in altitude) to obtain better resolution of near-surface processes. The Kain–Fritsch cumulus parameterization scheme was used with the 9-km grid, but the 3- and 1-km grids were allowed to represent cloud processes explicitly (Bélair and Mailhot 2001). The five-category ice microphysics scheme was used with inverse exponential size distribution $N(D) = N_0 \exp(-\lambda D)$; typical intercept parameters for a midlatitude storm were used: $N_0 = 0.08$, 0.03, and 0.0004 cm^{-4} for rain, snow, and hail, respectively. The densities for rain, snow, and hail were set to 1, 0.1, and 0.913 g cm^{-3}, respectively. This is a common microphysics parameterization that is used in some of the models used to build the GPROF algorithm cloud database (Kummerow et al. 2001).

2) WSR-88D OBSERVATIONS

Level-II data were used from the lowest elevation angle of the Fort Worth WSR-88D (KFWS) radar. These data were then remapped, by a quadratic interpolation scheme, to the ARPS grid within the spatial domain of the model. The effective reflectivity factor from observations (referred to simply as reflectivity) was analyzed throughout this study. WSR-88D data, consisting of 3D fields of reflectivity, were used for analysis of cloud profiles described in section 4. For quality control, the data were checked for unfolding, transient echoes in clear air were removed (images were despeckled), and the data were screened for anomalous propagation. Surface rainfall was computed directly from the WSR-88D lowest scan. Reflectivity Z was converted to rain rate R using a standard Z–R relationship $Z = 300R^{1.4}$ (Fulton et al. 1998). No vertical profile correction was applied.

A single missing-value flag was used to fill in 1) pixels that were out of the range of the radar, 2) values that were removed during quality-control procedures, or 3) values that were below the limits of detection of the radar (no echo returned). After careful consideration of both the lowest scan and 3D radar field, it was decided that the best treatment of these missing values was to set them to zero. This treatment is justified by the fact that the area analyzed is all within the range of the radar and quality control removes only a small number of values.

3. Surface rainfall: Modeled versus observed

a. Spatial and temporal domain

Before describing the comparison of the modeled and observed rainfall fields, some terminology used extensively throughout this paper is established. The term "field" is used to describe a set of observations or model outputs on an evenly spaced grid, similar to a digital image. The term "domain" refers to the areal extent of the analyzed field. "Grid spacing" refers to the distance between grid cells; it is the smallest grid size at which a field is available (sometimes also referred to as resolution). For brevity, the model with 1-km grid spacing may be referred to simply as the 1-km model.

The model outputs and radar observations with 1-km grid spacing were analyzed. Note that the "true" resolution of the WSR-88D observations varies with distance from the radar center because of beam spreading and that beyond the range of 60 km from the radar observations were interpolated to produce the 1-km gridded field. From the model domain, a subarea of

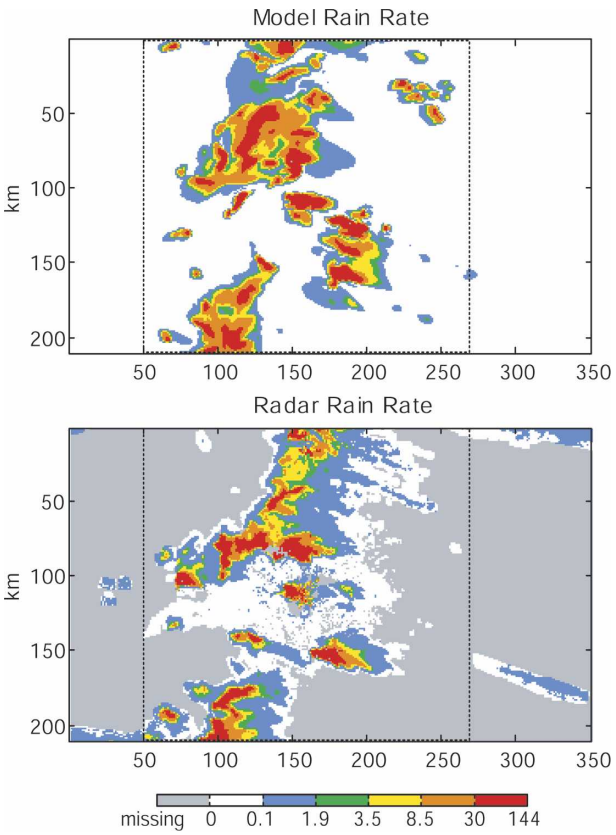

FIG. 3. Surface rain-rate images for the Fort Worth storm with 1-km grid spacing. The first frame (t = 0 min) is shown. The dotted lines outline the primary domain of analysis.

220×210 km^2 was selected for analysis (see Fig. 3). To follow the movement of the storm, we moved our "area of interest" from left to right, across the domain.

Atmospheric fields were computed every 5 min for the duration of the model run. A 1-h interval was selected for analysis, from 0000 UTC 29 March 2000 (t = 0 min) to 0100 UTC (t = 60 min), thus allowing for 0.5 h of spinup time for the 1-km model (see Fig. 2). The 13 time instants are referred to as frames throughout the remainder of this paper [i.e., t = 0 min (frame 1), t = 5 min (frame 2), . . . , t = 60 min (frame 13)]. Because the objective of this study was to evaluate the accuracy of modeled 3D hydrometeor fields rather than the accuracy of the forecast of weather events on the ground, statistics were calculated from atmospheric fields from a 1-h time window to minimize the effects of small differences in timing and location of storm development.

b. Basic statistics

A lower threshold of 0.1 mm h^{-1} and an upper threshold of 144 mm h^{-1} were applied to both the modeled and radar-observed rain-rate data. All values that were less than the lower threshold were set to zero, probably resulting in the removal of a portion of stratiform precipitation. All values that were greater than the upper threshold were set to the upper threshold to remove anomalously high precipitation values associated with hail (Fulton et al. 1998). Hail from this storm did reach the ground.

The time series of the basic statistics of the surface rain rate (including zeroes) are shown in Fig. 4. The percent area covered by rain is the fraction of pixels in the study area that have a nonzero (>0.1 mm h^{-1}) rain rate. The percent area covered in the modeled fields was found to be always greater than that corresponding to the radar-observed fields; this statistic is very dependent on the lower threshold and the spatial domain selected, however. The mean of the modeled rain rates was found to be greater than the mean of the radar rain rates, implying that the model is overpredicting the to-

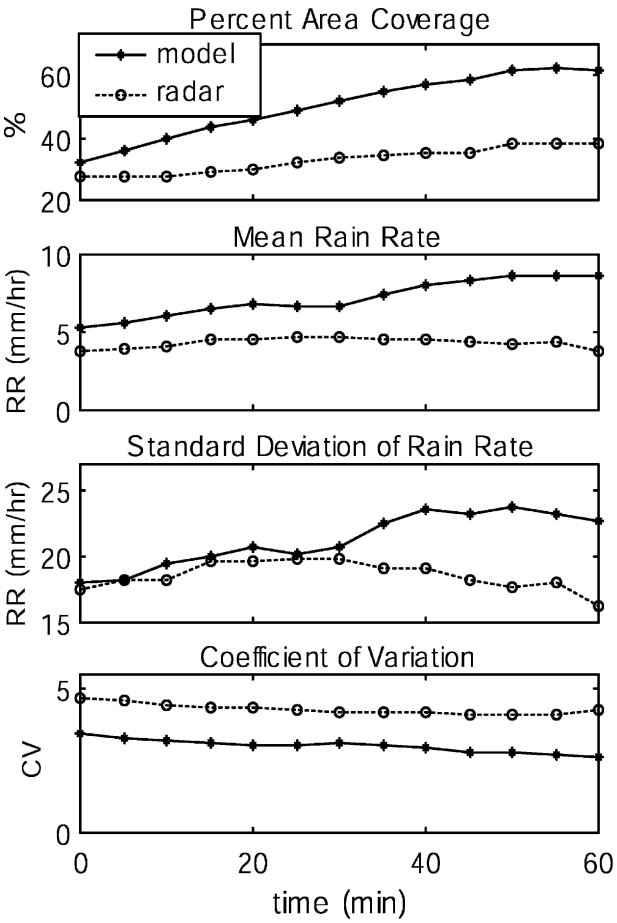

FIG. 4. Basic statistics of surface rain rate over the whole field (raining and nonraining pixels; see Fig. 3) for the Fort Worth storm with 1-km grid spacing. (top to bottom) The proportion of the domain covered by rain, the mean, the standard deviation, and the coefficient of variation.

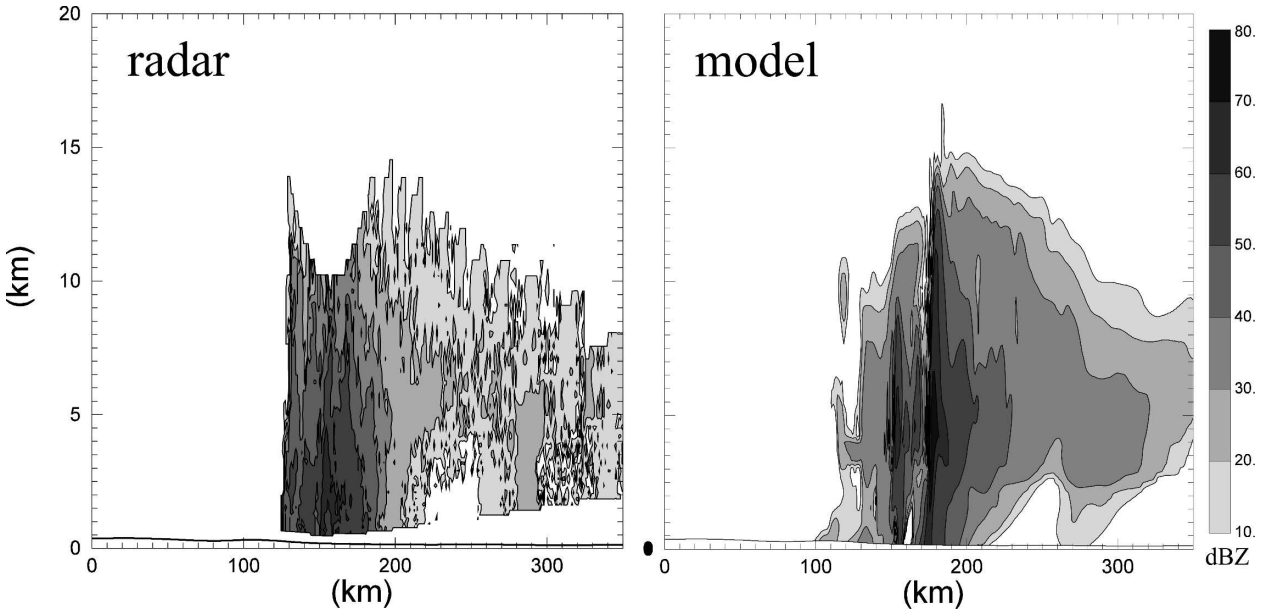

FIG. 5. Vertical profiles of reflectivity from (left) radar observations and (right) the model. The vertical slice is taken from the same location (at $y = 125$ km) from the seventh time frame ($t = 30$ min).

tal amount of rainfall over this time period. The model also generally predicted more spatial variability in the rainfall field, as measured by the standard deviation, in comparison with radar observations. However, if the coefficient of variation (standard deviation/mean) is used as a normalized measure of variability, the model was found to produce rain fields with reduced variability relative to observations. Note that all of these surface rain-rate statistics are dependent on 1) the choice of the spatial domain analyzed, 2) the value of the upper and lower thresholds, and 3) the treatment of the "missing values" in radar observations.

4. Reflectivity profiles: Modeled versus observed

a. Limitations with WSR-88D vertical profiles

Although WSR-88D provides good temporal coverage over a large area, there are limitations in its use to resolve the vertical structure of a cloud. Farther from the radar center, the vertical resolution of the radar beams deteriorates so that at a distance of 150 km from the radar center, the radar beams are between 2 and 3 km in width. Higher in the atmosphere, there are gaps between the radar beams, especially above 5-km altitude. In a 30-km radius around the radar, coverage does not extend to the top of the cloud. Also, radar reflectivity suffers from the same ambiguity discussed in section 3; that is, the missing-value flag includes data that are below limits of detection of the radar, data that were removed during quality control procedures, and data that were out of the spatial range of the radar. To minimize the effect of these missing data and for consistency with previous radar profile studies, only values greater than 0 dBZ were considered in both modeled and radar reflectivity fields. Despite these limitations with radar observations, we feel that some inferences from these data for the purposes of our study are still reasonable.

b. Reflectivity cross sections

Several features are apparent from the vertical cross sections of reflectivity from the model and radar observations shown in Fig. 5. A strong core of high reflectivity (>50 dBZ) that reaches the surface is present in both cross sections between 100 and 200 km. The core reaches maximum reflectivity slightly below the freezing level (~3.8 km) in the observations and slightly above the freezing level in the model. Also, the core extends up to about 9 km in the observations and up to about 13 km in the model, indicating high updraft velocities. Some of the limitations in the WSR-88D radar can be seen in the observations; there are missing data near the top of the cloud and near the bottom of the cloud that vary with the range from the radar. In both the observations and the model, the clouds are not significantly tilted with height—an observation that is important when considering profile statistics. Whereas these observations provide important qualitative infor-

mation about the performance of the model in approximating cloud processes, the statistics of reflectivity profiles tell a very different story.

c. Conditional reflectivity-profile statistics

A reflectivity profile is defined as a single vertical column of reflectivity values that extends from the lowest altitude directly up to the top level in the ARPS grid. These reflectivity profiles were grouped into five bins based on precipitation on the ground; that is, all profiles, from all 13 frames in the hour, with a given range of surface rain rate were considered together for analysis. Thus, the horizontal locations and specific timing of the data were ignored and the data were stratified by altitude only and separated into bins based on a single surface property (i.e., that of surface rain). Because the probability density functions of surface rain rates are not symmetric but heavily tailed (approximately lognormal), the bins were selected on the basis of equal probability of occurrence of surface rain within each bin (Table 1), thus guaranteeing an approximately equal number of profiles per bin.

Important differences are apparent between mean reflectivity profiles from the Fort Worth storm with 1-km grid spacing from model and radar observations (Fig. 6). Mean reflectivity near the surface (1-km height) is lower in the radar observations than in the model. Radar observed reflectivity values tend to decrease monotonically from the surface to the cloud tops. In contrast, model profiles have a "nose" with very high reflectivity values near the 0°C level. The modeled reflectivity values increase sharply to the 0°C level and then decrease sharply to the cloud top. This nose of high reflectivity in model reflectivity calculations may be caused by problems with hydrometeor concentrations or with the estimation of reflectivity from hydrometeor concentrations, which will be discussed in the next section. The nose of radar reflectivity near the 0°C level is in some ways similar to the radar brightband that appears in stratiform precipitation from melting snow. In the case of the Fort Worth model, however, the nose appears to be primarily caused by hail.

TABLE 1. Rain-rate bin thresholds used for reflectivity profile analysis.

Bin	Lower rain rate (mm h^{-1})	Upper rain rate (mm h^{-1})
1	1.00	1.88
2	1.88	3.50
3	3.50	8.50
4	8.50	30.00
5	30.00	144.00

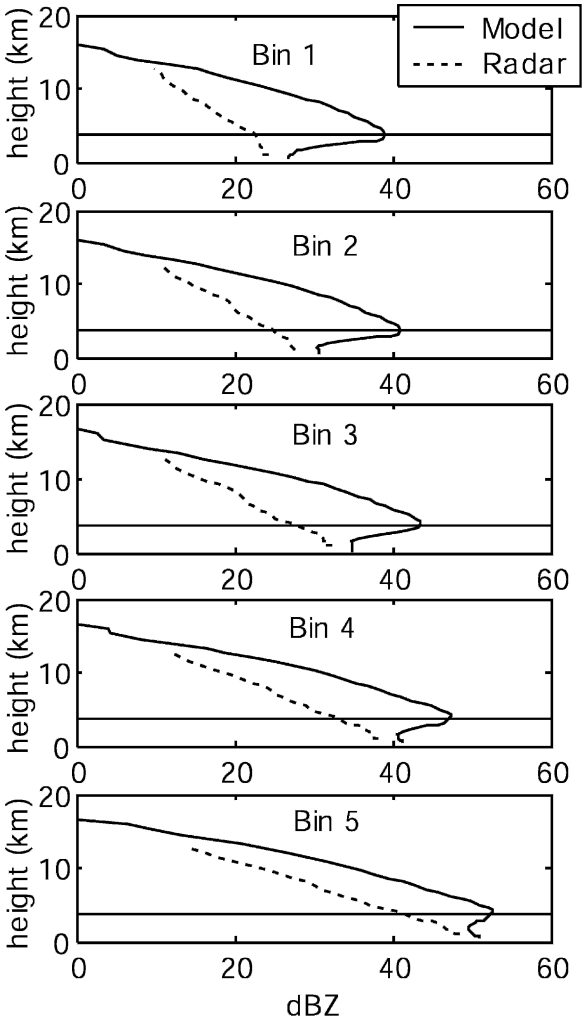

FIG. 6. Comparison of modeled (solid lines) and observed (dashed lines) mean reflectivity profiles from the Fort Worth storm with 1-km grid spacing conditional on surface rain rate subclassified according to magnitude into five different bins (see Table 1 for bin thresholds). The horizontal line represents the mean freezing level.

The mean reflectivity lapse rate above the freezing level, defined as the rate of decrease in reflectivity as height increases (Table 2), is comparable between the model and the radar observations. These values are also comparable to those observed by radar in previous

TABLE 2. Mean reflectivity lapse rate (the rate of decrease in reflectivity with increasing height; dBZ km^{-1}) from the 0°C level (3.8-km height) to the −20°C level (7.0-km height).

	Bin 1	Bin 2	Bin 3	Bin 4	Bin 5
Model	2.0	2.1	2.3	2.7	3.0
Radar	1.5	1.5	1.7	2.7	3.0

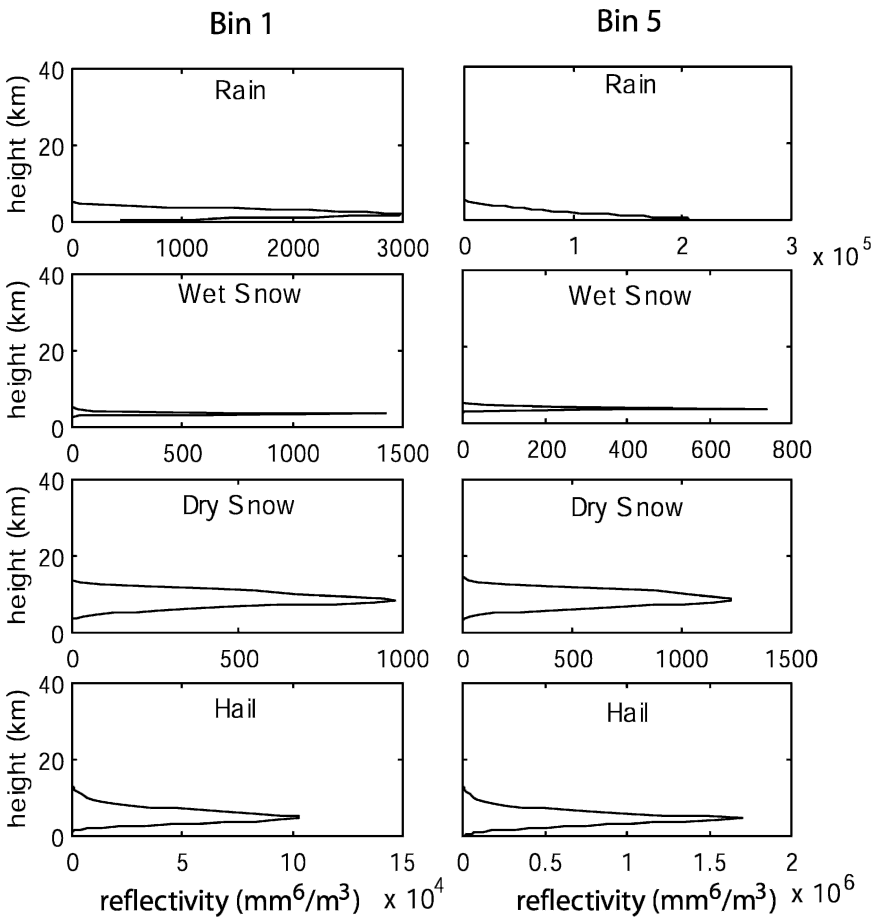

FIG. 7. Contribution to reflectivity profiles from each of the hydrometeor components (rain, wet snow, dry snow, and hail) for the Fort Worth storm with 1-km grid spacing for the first time frame. In each grid cell, the four reflectivity values were added together and then reported in a log scale (dBZ units). The mean profiles conditional on surface rain-rate amounts within bins (left) 1 and (right) 5 are shown.

studies. Steiner et al. (1995) reported a lapse rate of 2.5 dBZ km^{-1} for a monthlong average dataset from Darwin, Australia; the value was the same for convective and stratiform precipitation. Zipser and Lutz (1994) reported a rate of 1.5 dBZ km^{-1} for strong convective cells observed in Oklahoma during the Oklahoma–Kansas Preliminary Regional Experiment for Storm-scale Operational and Research Meteorology-Central (OK PRE-STORM) field campaign. They also derived rates of 2.0 dBZ km^{-1} from a New England rainstorm and 1.3 dBZ km^{-1} from a New England hailstorm as reported by Donaldson (1961). However, the rates from Zipser and Lutz (1994) are not directly comparable to those reported here, because they come only from the strongest convective cores and are from the median profile instead of the mean. The differences in lapse rates reported in Table 2 are related mostly to the low-level reflectivity in each group.

d. Sensitivity of reflectivity to hydrometeor assumptions

1) SENSITIVITY TESTS ON HYPOTHETICAL CLOUD PARAMETERS

Raleigh scattering theory is used to predict the radar reflectivity that would be observed given a modeled 3D hydrometeor field and assumptions about its back scattering. Details of these calculations are given in the appendix. Using these calculations, the reflectivity profiles can be broken down to look at the mean contribution from rain, wet snow, dry snow, and hail to the modeled reflectivity profiles (Fig. 7). These mean profiles suggest that reflectivity from hail and snow is probably the cause of the large nose observed in the overall mean profiles shown in Fig. 6 and that snow is the only species with significant reflectivity near the top of the cloud.

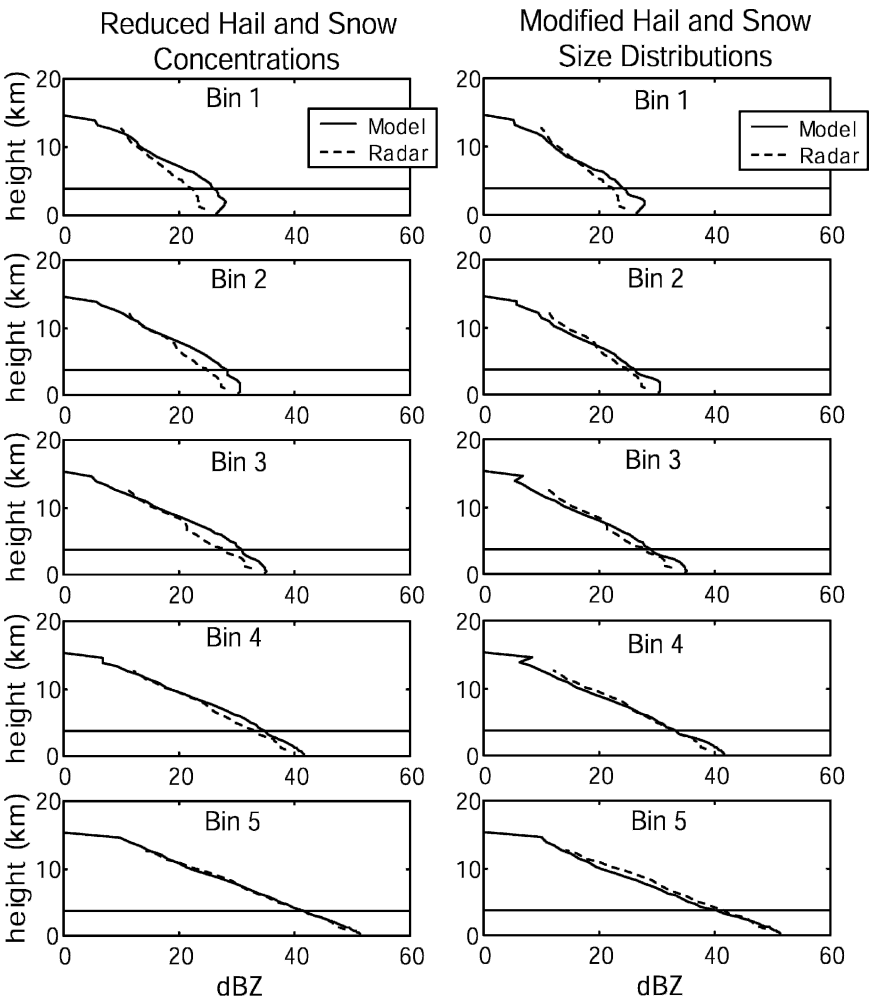

FIG. 8. Alternative modeled reflectivity profiles created by (left) reducing the concentration of hail and snow and (right) increasing the intercept parameter of the size distribution for hail and snow. Profiles are conditioned on rain rate, which is subclassified according to magnitude into five different bins (see Table 1 for bin thresholds). The horizontal line represents the mean freezing level.

To investigate the effect of hail and snow on reflectivity profiles further, reflectivity calculations were modified and the resulting profiles were plotted in Fig. 8. Two modifications were used. In modification 1, the size distribution of hail and snow was modified to reduce the number of large particles by setting $N_{0s}^* = 100N_{0s}$ and $N_{0h}^* = 100N_{0h}$, where N_{0h} and N_{0h} are the intercept parameters of the size distribution of snow and hail, respectively. In modification 2, the mixing ratio of hail and snow was decreased by setting $q_s^* = q_s/10$ and $q_h^* = q_h/10$, where q_s and q_h are the mixing ratios of hail or snow, respectively.

Modification 1 is motivated by the fact that the assumed (original) size distributions for hail and snow produce too many large particles, particularly hailstones, which results in high reflectivity values. Modification 1 is equivalent to multiplying the hail and snow reflectivity by a factor of $(1/100)^{3/4} \approx 1/30$ [see Eqs. (A2), (A3a), and (A3b) in the appendix]. Modification 2 is motivated by the fact that the model overpredicts the mixing ratio of hail and snow, by 1) transferring too much water from the surface into the atmosphere, 2) converting too much liquid water or water vapor to hail and snow, or 3) overestimating the ice in fields used as the initial condition. Modification 2 is equivalent to multiplying the reflectivity by a factor of $(1/10)^{7/4} \approx 1/60$. Although these modifications to the composition of the modeled atmosphere are not based on knowledge of the microphysics of the actual storm, they are guided by knowledge of the direct effect that these variables have on reflectivity calculations (see the equations in the appendix).

Modifying the size distribution of hail and snow has the effect of reducing the number of large hailstones and snowflakes, thus reducing reflectivity. The original size distribution and density of hail are typical of midlatitude convective clouds, whereas the modified size distribution is more typical of graupel in warm-frontal clouds (although it would be accompanied by lower-density particles; Tao and Simpson 1993). Modifying the size distribution in the microphysical parameterization scheme within ARPS would also have an important impact on ice processes and the thermodynamics of the model as well as on the terminal velocities of the precipitating hydrometeors—thus modifying the modeled rain rate. Note that there is significant uncertainty in the size distribution of hail/graupel in the first place (Fovell and Ogura 1988). Field studies that have looked at hailstones found on the ground after midcontinental storms have found significant variation in the intercept parameter of the fitted exponential distribution from storm to storm (Knight et al. 1982), and some have found that a three-parameter gamma distribution gives a better fit and estimates fewer large hailstones (Ziegler et al. 1983). Model reflectivity calculations are also sensitive to uncertainties in snow and hail density, a quantity that is very difficult to measure directly.

The resulting mean reflectivity profiles from using these modifications are shown in Fig. 8. It is seen that the reflectivity computed from the modified cloud structures agrees with the observed reflectivity and that the nose found previously in modeled reflectivity profiles has disappeared. This sensitivity analysis, despite its limitations, points to the possibility of having too much hail in the modeled clouds. The implication of a possible mismatch between modeled and observed cloud hydrometeors is important for the performance of the inversion algorithm (GPROF) and warrants further study.

2) AN ALTERNATIVE ICE MICROPHYSICS SCHEME

To assess the impact of different microphysics schemes on the modeled cloud structure, an alternative 1-km simulation was conducted using the Rutledge and Hobbs (1984) microphysics parameterization scheme. Both the Lin scheme (Lin et al. 1983) and the Rutledge–Hobbs (RH) scheme are three-class ice schemes. Besides some formulation differences, the major difference between the two is the ice classification: the Lin scheme uses cloud ice–snow–hail whereas the RH scheme uses cloud ice–snow–graupel, in which the graupel has a larger intercept parameter and smaller density and thus falls much slower. Based on this feature, the Lin scheme is considered to be more suitable for hail-bearing central U.S. thunderstorms and the RH scheme is more suitable for tropical squall lines and midlatitude cold-frontal rainbands with extensive trailing anvil (with a bright band). The Fort Worth tornadic thunderstorm used in this study reported softball-sized hail. Thus, the Lin scheme should be appropriate in nature. That said, it is useful to compare the modeled cloud structures between the two schemes. Therefore, the model was rerun with the Lin microphysics scheme but with the RH graupel parameters (intercept parameter of 0.04 cm^{-4} and density of 0.4 g cm^{-3}), and an accordingly adjusted terminal velocity. This is equivalent to experiment D in the study by McCumber et al. (1991), which demonstrated that by replacing hail/graupel parameters in the Lin scheme most of the modeled cloud features with the RH scheme can be obtained.

The resulting storm cells show more graupel remaining in the midcloud layer with much less reaching the ground, reflecting the fact that graupel particles are smaller in size and fall much slower (figures not shown). This change, however, does not lead to a better agreement with the radar profiles. Figure 9 shows the mean reflectivity profiles from the model with the two different size distributions and densities. Although there are some differences between the mean profiles, the fundamental problem of high reflectivity near the freezing level remains unchanged. Although the graupel intercept parameter is the same as in modification 1, the mean profile is nothing like that in Fig. 8 (right panels) given that the reduced particle density cancels a big part of the reduction in reflectivity resulting from the increase in the intercept parameter [see Eq. (A4)]. This result suggests that the problem of disagreement between reflectivity profiles may not be properly solved with the current three-class ice schemes. More comprehensive ice schemes, such as four class with both graupel and hail and their size distributions explicitly predicted by models, might be required (e.g., Ferrier 1994). It may also be that the problem may be attributable to some other part of the physical model, such as a bias in the surface energy and moisture budget.

e. Contoured Frequency by Altitude Diagrams (CFADs)

The mean reflectivity profiles give information about the average behavior of reflectivity, but CFADs can show the probability distribution at every height [see Yuter and Houze (1995) for a complete description of CFADs]. In a procedure similar to that used to create profile statistics, spatial locations of the data were ignored and the data were stratified based only on alti-

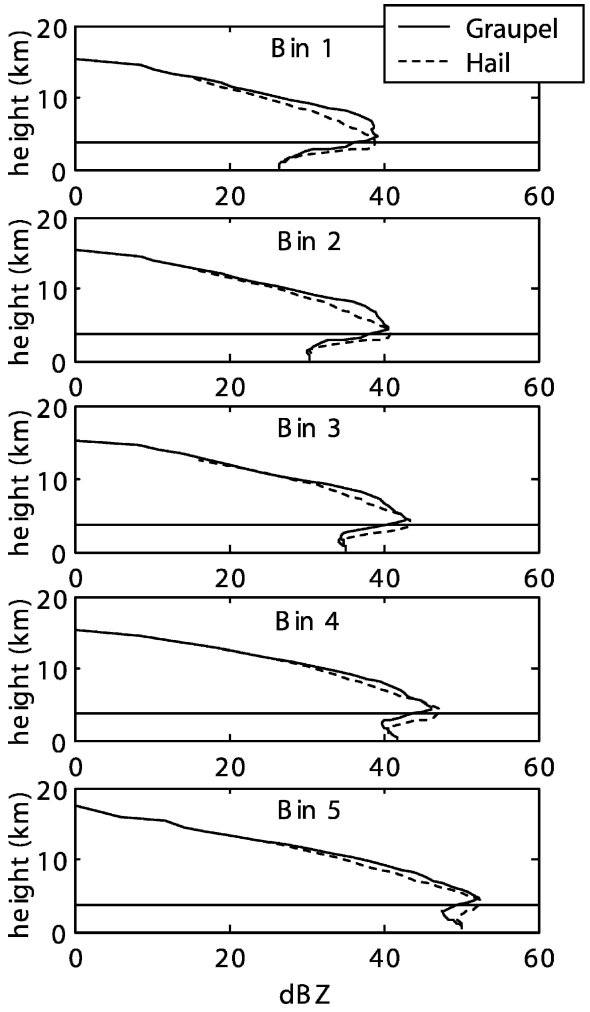

FIG. 9. Comparison of modeled mean reflectivity profiles conditional on surface rain rate from the ARPS model with microphysical parameters for hail (dashed line) and for graupel (solid line) for the Fort Worth storm with 1-km grid spacing. Profiles are conditioned on rain rate, which is subclassified according to magnitude into five different bins (See Table 1 for bin thresholds). The horizontal line represents the mean freezing level.

tude. To create the CFADS, a probability distribution of reflectivity values was created at each altitude using 4-dBZ bin increments; only reflectivity values greater than 0 dBZ (1 mm^6 m^{-3}) were considered. The histograms were normalized by the number of nonmissing reflectivity values at that level and then multiplied by 100 to represent the fraction as a percent (see Fig. 10). All probability distributions were then lined up in order of altitude to create a surface that was then contoured for a simplified 2D presentation. A CFAD of reflectivity was created for all raining pixels (Fig. 11) and then conditional on each of the five surface rain-rate bins listed in Table 1 (Fig. 12).

The median lines in the conditional CFADs in Fig. 12 (shown as dashed white lines) reveal a structure that is similar to that of the mean reflectivity profiles shown in Fig. 6, with the modeled profiles exhibiting a maximum of high reflectivity near the freezing level while the radar profiles decrease monotonically from the ground to the top of the cloud. The reflectivity distributions in the CFADs appear to be unimodal throughout but sometimes are negatively skewed. The widths of the distributions are comparable (modeled vs observed) at low rain rates. At higher rain rates, the distributions of modeled reflectivity are narrower. Differences in distribution widths have been related to differences in the types of clouds present, with wider distributions being more associated with convective precipitation and narrower distributions being associated with stratiform precipitation (Yuter and Houze 1995).

Although no other model studies of midlatitude convective storms that look at reflectivity profile statistics have been found in the literature, a recent study by Braun (2006) did compare modeled and TRMM PR observed reflectivity CFADs from Hurricane Bonnie. They also found that the model overpredicted high reflectivity values at all levels and concluded that, if the hydrometeor size distributions are correct, the reflectivity overestimation can be attributed to overestimation of hydrometeors at all levels. Braun (2006) pointed out that while it may seem logical to attribute these discrepancies to a problem with the microphysical parameterization scheme, it could also result from a positive bias in boundary layer temperature and vapor mixing ratio. Thus, as discussed in an earlier study by Braun and Tao (2000), the overproduction of precipitation may be the result of the boundary layer parameterization rather than the microphysical parameterization. In addition, the Fort Worth model was started up by a radar data assimilation scheme that adds water and ice hydrometeors to the cloud. It may be that too much water was added to the cloud in this cycle or that the 3-km resolution was too coarse so that the hydrometeors were spread over too-large areas (Xue et al. 2003).

Yuter and Houze (1995) used CFADs to study the development of a storm and the associated transformation from primarily convective precipitation to more stratiform precipitation. A similar evolution can be seen in our analysis by looking at the time progression in CFADs at single time frames during the course of 1 h of the Fort Worth storm being considered (Fig. 13). The temporal changes can be seen more clearly in the upper portion of the CFADs because they are effectively separated by reflectivity on the ground. At the beginning of the hour, the CFADs tend to be wide and not clearly unimodal, if not multimodal. As the storm matures, the distributions narrow and the strong diago-

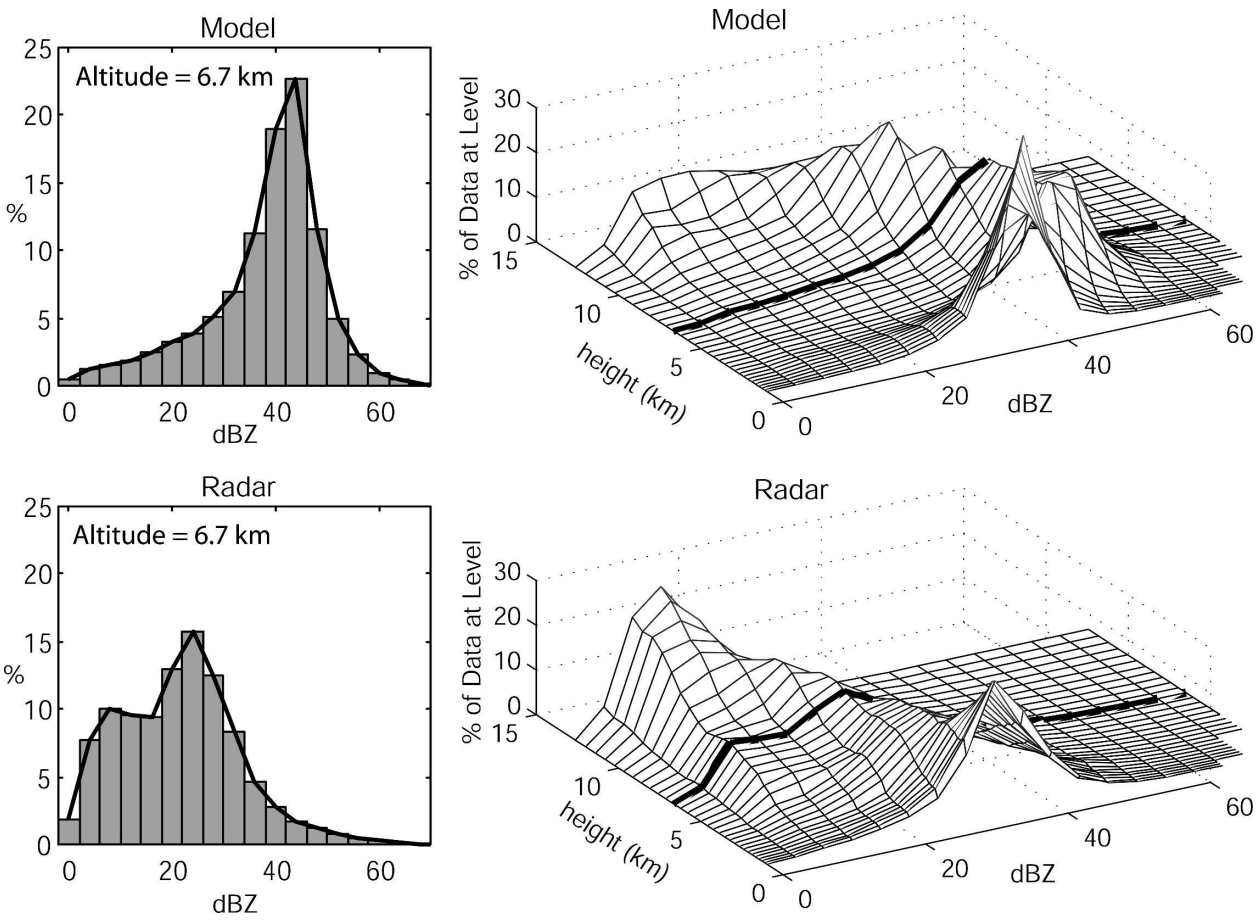

FIG. 10. (left) Example probability distributions for (top) modeled and (bottom) radar-observed reflectivity, from 6.7-km altitude. (right) Surfaces of probability diagrams from all heights. CFADs are created by first plotting a probability diagram for reflectivity at each height and then arranging the probability diagrams in order from the lowest to highest altitude to create a surface. This surface is contoured to create the CFAD. The dark line on the surface represents the contribution of the probability distribution at 6.7-km altitude to the surface.

nal profile becomes more apparent. The reduced slope of the median line indicates more efficient growth of precipitation particles and/or slower fall speeds. Although the precipitation may still be primarily convective in nature, the precipitation formation mechanism is probably changing toward the slowly falling snow particles in the upper cloud, associated with stratiform precipitation.

5. Conclusions and future research

The goal of this research was to investigate the statistical structure of hydrometeor fields predicted by cloud-resolving models and to provide an assessment of how well CRMs can reproduce the vertical structure of observed storms. The motivation for this research was twofold. First, the ability of CRMs to produce realistic cloud hydrometeor profiles has direct implications in inversion-type precipitation retrieval algorithms, such as the GPROF algorithm used with passive microwave sensors (see Kummerow et al. 2001 and references therein). Second, quantitative precipitation forecasting from numerical weather prediction models is directly affected by the representation of hydrometeors within the cloud, and further improvement in QPF may be limited by the ability of the models to reproduce storms with realistic vertical structure.

The ARPS model with explicit microphysics and 1-km grid spacing was used as the cloud-resolving model to forecast a severe midlatitude storm over Fort Worth. Radar observations of the same storm allowed for a comparison of modeled and observed vertical hydrometeor structure indirectly through comparison of modeled and observed vertical reflectivity profiles. The major findings of this research are outlined below.

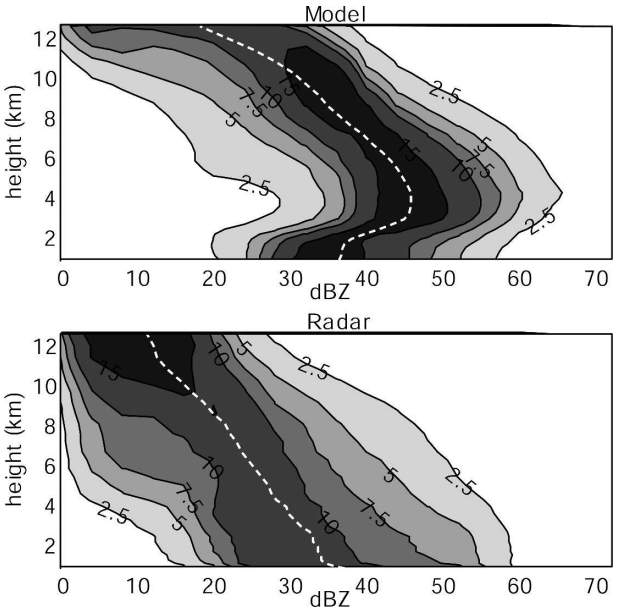

FIG. 11. CFAD of reflectivity from the Fort Worth storm with 1-km grid spacing for all raining profiles. Reflectivity profiles from all raining pixels were accumulated over the entire hour, and CFADs were created with a bin size of 4 dB*Z*. The median is shown as a white dashed line.

- For the storm studied, the ARPS model run at 1-km resolution overpredicted the surface rain rate and its standard deviation (Fig. 5). However, it underestimated the variability of surface rainfall, as measured by the coefficient of variation, but the differences were very small (<20%).
- The modeled hydrometeor profiles resulted in an overestimation of the above-surface reflectivity and exhibited a nose (i.e., an abrupt increase in reflectivity) that peaked at the freezing level and that was not seen in radar observations (Fig. 6). This overestimation can be explained by overproduction of hail and snow in modeled hydrometeor fields or incorrect hydrometeor size distribution assumptions in the model (Fig. 8). However, incorporating changes to the size distribution into the CRM itself did not significantly alter the shape of mean reflectivity profiles (Fig. 9). Thus, it may be concluded that there is an overproduction of hail and/or graupel around the freezing level in the model.
- The temporal evolution of both modeled and observed CFADs exhibited some diagonalization, indicating a transition from primarily convective rain processes to more stratiform rain processes (Fig. 13).

The disagreement identified in our study between modeled and observed cloud structure is expected to have significant implications for rainfall retrievals with the TRMM GPROF algorithm (Kummerow et al. 2001) and the modified GPROF algorithm (Shin and Kummerow 2003) investigated for the proposed Global Precipitation Measuring (GPM) Mission, because these algorithms depend on the results of cloud models, similar to the ARPS, to construct a cloud database. In tests of the parametric retrieval method proposed for the GPM mission, Shin and Kummerow (2003) also found evidence that the CRMs used to build the cloud database overpredicted the amount of ice or the size of ice particles in the cloud. A comparison of brightness temperatures observed by the TRMM Microwave Imager with those retrieved from the cloud database showed that scattering by ice was generally overpredicted in modeled fields.

This study inferred discrepancies between modeled and observed clouds indirectly by comparing the 3D reflectivity fields. To compare modeled hydrometeor profiles directly and to isolate the cause of the disagreement between modeled and observed reflectivity profiles, multipolarimetric radar observations could be used to provide more information about observed hydrometeor fields. Uncertainties resulting from limited spatial resolution and gaps in the vertical coverage by volume-scanning radar could be resolved by using observations from a vertically pointing radar that would provide better vertical resolution but less spatial coverage than the WSR-88D. Also, observations from multiple volume-scanning radars would eliminate some of the radar artifacts, especially the cone of silence about the single radar used in this study. In addition, 3D radiative transfer calculations through the modeled and observed cloud atmospheres would provide further insight into how differences in the spatial statistics of hydrometeor fields would be reflected in observed brightness temperature and, ultimately, in passive microwave rainfall retrieval. For the particular storm analyzed, which was captured well by the model, it was unnecessary to subclassify the modeled and observed cloud structures through criteria other than surface rain; however, subclassification (e.g., convective/stratiform, ice/no ice) might be necessary for other systems.

To recommend improvements to cloud-resolving models, a sensitivity analysis should be performed to assess the impact of modifying the microphysical parameterization schemes, hydrometeor size distributions, and surface parameterization schemes on hydrometeor profiles. The issues are certainly not straightforward and have been under investigation for many years. Although more-sophisticated microphysical parameterization schemes have been developed (Meyers et al. 1992; Ferrier 1994), their use in numeri-

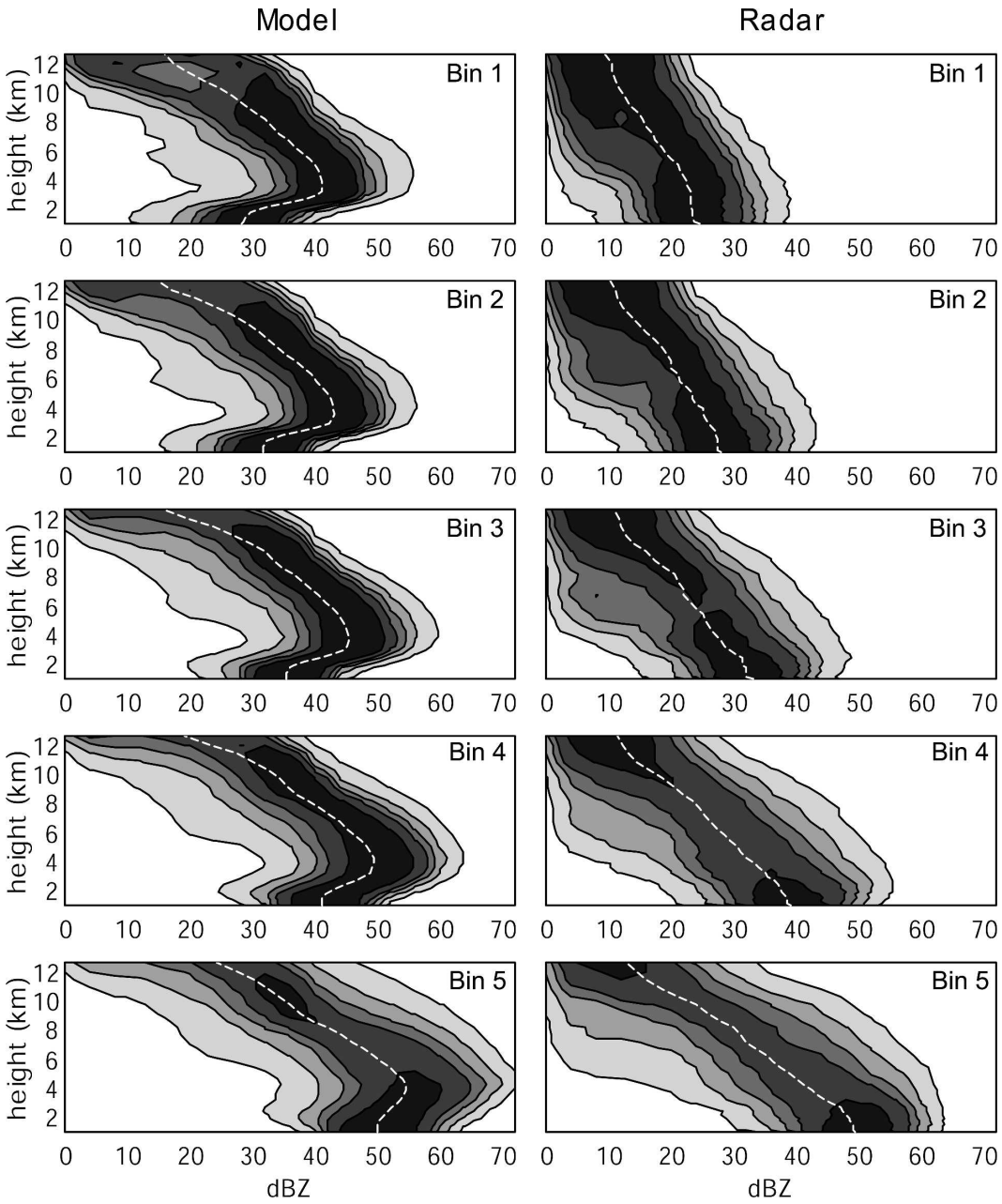

FIG. 12. Same as in Fig. 11, but reflectivity profiles from all raining pixels were accumulated over the entire hour conditional on surface rain rate (see Table 1 for bin thresholds) and CFADs were created with a bin size of 4 dB*Z*. Contours depict the 2.5%, 5%, 7.5%, 10%, and 15% probability levels, and the median is shown as a white dashed line.

cal weather models has been limited because they are too computationally expensive. Realistic hydrometeor profiles may not be required for every application, but they do lend confidence to precipitation forecasts. Assessing the performance of a numerical weather prediction model by studying only how well it reproduces surface rainfall does not preclude cases in which one gets the right answer for the wrong reason, thus diminishing confidence that the model will perform as well in other situations. This reason is why "physical validation" studies, such as the one performed here for the assessment of both numerical weather prediction models and satellite rainfall retrievals, are important and complementary to more statistically oriented comparisons of surface precipitation (Zepeda-Arće et al. 2000). Any numerical weather prediction model will probably

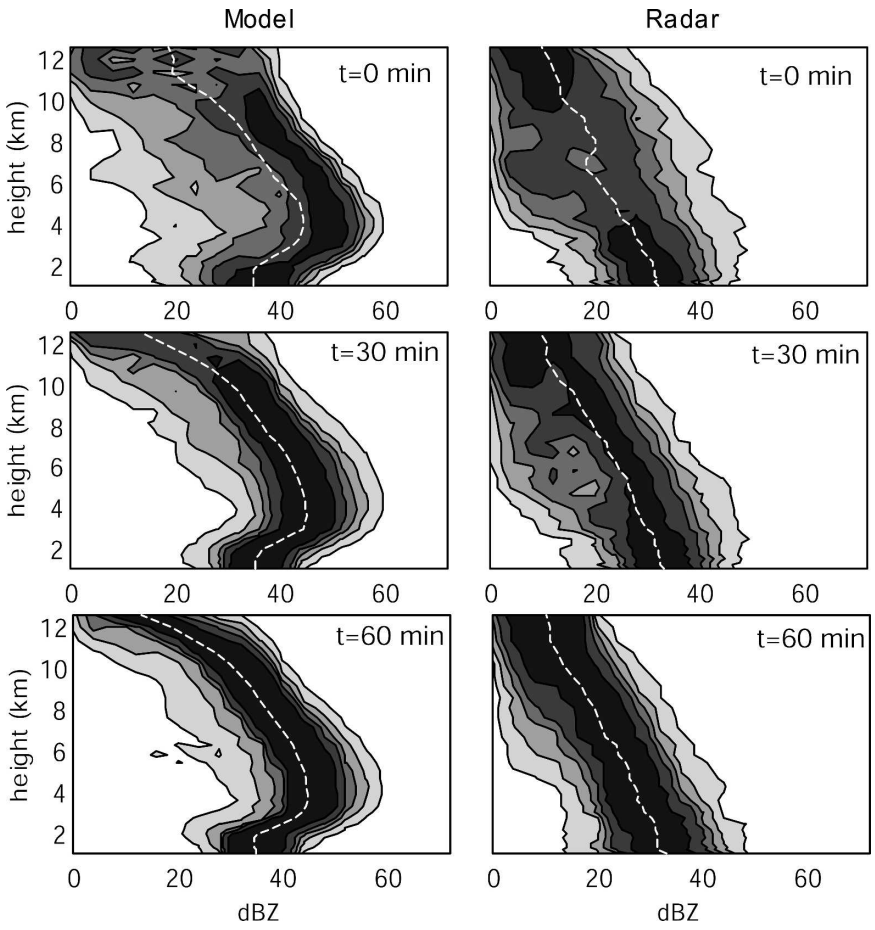

FIG. 13. CFADs of reflectivity from three time frames of the Fort Worth storm with 1-km grid spacing for bin 3: $3.5 <$ rain rate ≤ 8.5 mm h^{-1}. Contours depict the 2.5%, 5%, 7.5%, 10%, and 15% probability levels, and the median is shown as a white dashed line.

be limited by the performance of microphysical or surface parameterization schemes, and further improvements will have to start with understanding of how best to reproduce the hydrometeor fields above the surface, and not only the surface rain.

Acknowledgments. This research was funded by NASA Grants NAG5-12909 and NAG5-13639 to Foufoula-Georgiou and NSF Grant ATM-0130394 to Foufoula-Georgiou and Droegemeier. Computer resources were provided by the Minnesota Supercomputer Institute Digital Technology Center at the University of Minnesota. ARPS model simulations were conducted on the University of Oklahoma Supercomputing Center for Education and Research (OSCER) Pentium Xeon Linux cluster. All of this support is gratefully acknowledged. We are also grateful for the many helpful suggestions that were provided by Dr. Sandra Yuter of the University of Washington.

APPENDIX

Reflectivity Calculations

In ARPS, hydrometeor mixing ratios, size distributions, and densities are used to estimate the reflectivity that would be observed by a radar that is scanning the predicted cloud atmospheres. This calculation is based on Rayleigh scattering, assuming a Marshall–Palmer-type exponential size distribution as outlined by Smith et al. (1975) and Ferrier (1994). The Marshall–Palmer-type size distribution for a given hydrometeor species i is defined as

$$N = N_{0i} \exp(-\lambda D),$$

where N_{0i} is the intercept parameter, λ is the slope parameter for the inverse exponential distribution, and D is the diameter of the particles. The slope parameter is a function of the intercept parameter so that the den-

TABLE A1. Description of constants and variables used to estimate the radar reflectivity from model-predicted atmospheric fields.

Symbol	Definition	Numerical value	Units
k	Unit conversion factor	1×10^{18}	$(1000\ \text{mm}/1\ \text{m})^6$
N_{0s}	Intercept of snow size distribution	3.0×10^6	m^{-4}
N_{0h}	Intercept of graupel/hail size distribution	4.0×10^4	m^{-4}
N_{0r}	Intercept of rain size distribution	8.0×10^6	m^{-4}
q_s	Mixing ratio of snow	Model predicted	kg (kg of air)$^{-1}$
q_{s+}	Mixing ratio of wet snow	Model predicted	kg (kg of air)$^{-1}$
q_{s-}	Mixing ratio of dry snow	Model predicted	kg (kg of air)$^{-1}$
q_h	Mixing ratio of hail	Model predicted	kg (kg of air)$^{-1}$
q_r	Mixing ratio of rain	Model predicted	kg (kg of air)$^{-1}$
ρ	Density of air	Model predicted	kg m^{-3}
T	Temperature	Model predicted	°C
ρ_s	Density of snow	100	kg m^{-3}
ρ_h	Density of hail	913	kg m^{-3}
ρ_r	Density of rain	1000	kg m^{-3}
ρ_{ice}	Density of pure ice	917	kg m^{-3}
$\lvert K\rvert_i^2$	Dielectric factor for ice	0.176	
$\lvert K\rvert_w^2$	Dielectric factor for water	0.93	

sity of hydrometeors remains constant with changes to the size distribution,

$$\lambda = \left(\frac{\pi N_{0i}\rho_i}{q_i\rho}\right)^{1/4},$$

where ρ_i is the density of the hydrometeor species, ρ is the density of the air, and q_i is the mixing ratio of each of the hydrometeor species.

The equations for estimating effective reflectivity factor (called reflectivity throughout) from the modeled atmosphere are outlined below:

$$Z_e = Z_r + Z_s + Z_h, \tag{A1}$$

$$Z_r = \frac{k720}{\pi^{7/4}N_{0r}\rho_r^{7/4}}(\rho q_r)^{7/4}, \tag{A2}$$

$$Z_{s-} = \frac{\lvert K\rvert^2_{\text{water}}}{\lvert K\rvert^2_{\text{ice}}}\frac{k720\rho_s^{1/4}}{\pi^{7/4}N_{0s}\rho_{\text{ice}}^2}(\rho q_{s-})^{7/4}, \tag{A3a}$$

$$Z_{s+} = \frac{k720}{\pi^{7/4}N_{0s}\rho_s^{7/4}}(\rho q_{s+})^{7/4}, \quad \text{and} \tag{A3b}$$

$$Z_h = \left(\frac{k720}{\pi^{7/4}N_{0h}\rho_h^{7/4}}\right)^{0.95}(\rho q_h)^{1.6625}. \tag{A4}$$

The constants and variables in the equations above are described in Table A1. Note that reflectivity from snow is divided into two components: Z_{s+} is due to wet snow (any snow below the freezing level) and Z_{s-} is due to dry snow (any snow above the freezing level). In Eq. (A1), Z_e is in units of millimeters to the sixth power divided by meters cubed and is reported on a log scale $\text{dB}Z = 10\log_{10}Z_e$.

REFERENCES

Adler, R. F., C. Kummerow, D. Bolvin, S. Curtis, and C. Kidd, 2003: Status of TRMM monthly estimates of tropical precipitation. *Cloud Systems, Hurricanes, and the Tropical Rainfall Measuring Mission (TRMM): A Tribute to Dr. Joanne Simpson, Meteor. Monogr.*, No. 51, Amer. Meteor. Soc., 223–234.

Bélair, S., and J. Mailhot, 2001: Impact of horizontal resolution on the numerical simulation of a midlatitude squall line: Implicit versus explicit condensation. *Mon. Wea. Rev.,* **129,** 2362–2376.

Berg, W., C. Kummerow, and C. A. Morales, 2002: Differences between east and west Pacific rainfall systems. *J. Climate,* **15,** 3659–3672.

Braun, S. A., 2006: High-resolution simulation of Hurricane Bonnie (1998). Part II: Water budget. *J. Atmos. Sci.,* in press.

——, and W.-K. Tao, 2000: Sensitivity of high-resolution simulations of Hurricane Bob (1991) to planetary boundary layer parameterizations. *Mon. Wea. Rev.,* **128,** 3941–3961.

Brewster, K., 1996: Implementation of a Bratseth analysis scheme including Doppler radar. Preprints, *15th Conf. on Weather Analysis and Forecasting*, Norfolk, VA, Amer. Meteor. Soc., 92–95.

——, 2002: Recent advances in the diabatic initialization of a non-hydrostatic numerical model. Preprints, *21st Conf. on Severe Local Storms/15th Conf. on Numerical Weather Prediction/19th Conf. on Weather Analysis and Forecasting*, San Antonio, TX, Amer. Meteor. Soc., CD-ROM, J6.3.

——, 2003: Phase-correcting data assimilation and application to storm-scale numerical weather prediction. Part II: Application to a severe storm outbreak. *Mon. Wea. Rev.,* **131,** 493–507.

Cifelli, R., and S. A. Rutledge, 1998: Vertical motion, diabatic heating, and rainfall characteristics in north Australia convective systems. *Quart. J. Roy. Meteor. Soc.,* **124,** 1133–1162.

——, W. A. Petersen, L. D. Carey, S. A. Rutledge, and M. A. F. da Silva Dias, 2002: Radar observations of the kinematic, microphysical, and precipitation characteristics of two MCSs in TRMM LBA. *J. Geophys. Res.,* **107,** 8077, doi:10.1029/2000JD000264.

Donaldson, R. J. J., 1961: Radar reflectivity profiles in thunderstorms. *J. Meteor.,* **18,** 292–305.

Ferrier, B. S., 1994: A double-moment multiple-phase four-class bulk ice scheme. Part I: Description. *J. Atmos. Sci.,* **51,** 249–280.

——, W.-K. Tao, and J. Simpson, 1995: A double-moment multiple-phase four-class bulk ice scheme. Part II: Simulations of convective storms in different large-scale environments and comparison with other bulk parameterizations. *J. Atmos. Sci.,* **52,** 1001–1033.

Fovell, R. G., and Y. Ogura, 1988: Numerical simulation of a midlatitude squall line in two dimensions. *J. Atmos. Sci.,* **45,** 3846–3879.

Fritsch, J. M., and R. E. Carbone, 2004: Improving quantitative precipitation forecasts in the warm season: A U.S.WRP research and development strategy. *Bull. Amer. Meteor. Soc.,* **85,** 955–965.

——, and Coauthors, 1998: Quantitative precipitation forecasting: Report of the eighth prospectus development team, U.S. Weather Research Program. *Bull. Amer. Meteor. Soc.,* **79,** 285–299.

Fu, Y., and G. Liu, 2001: The variability of tropical precipitation profiles and its impact on microwave brightness temperatures as inferred from TRMM data. *J. Appl. Meteor.,* **40,** 2130–2143.

Fulton, R. A., J. P. Breidenbach, D. J. Seo, D. A. Miller, and T. O'Bannon, 1998: The WSR-88D rainfall algorithm. *Wea. Forecasting,* **13,** 377–395.

Halverson, J. B., T. Rickenbach, B. Roy, H. Pierce, and E. R. Williams, 2002: Environmental characteristics of convective systems during TRMM–LBA. *Mon. Wea. Rev.,* **130,** 1493–1509.

Kain, J., and J. M. Fritsch, 1993: Convective parameterization for mesoscale models: The Kain–Fritsch scheme. *The Representation of Cumulus Convection in Numerical Models,* K. Emanuel and D. Raymond, Eds., Amer. Meteor. Soc., 678–684.

Kessler, E., 1969: *On the Distribution and Continuity of Water Substances in Atmospheric Circulation. Meteor. Monogr.*, No. 32, Amer. Meteor. Soc., 84 pp.

Knight, C. A., W. A. Cooper, D. W. Breed, I. R. Paluch, P. L. Smith, and G. Vali, 1982: Microphysics. *Hailstorms of the Central High Plains*, C. A. Knight and P. Squires, Eds., Colorado Associated Press, 151–193.

Kong, F., K. Droegemeier, V. Venugopal, and E. Foufoula-Georgiou, 2004: Application of scale-recursive estimation to ensemble forecasts: A comparison of coarse and fine resolution simulations of a deep convective storm. Preprints, *20th Conf. on Weather Analysis and Forecasting/16th Conf. on Numerical Weather Prediction,* Seattle, WA, Amer. Meteor. Soc., CD-ROM, P3.8.

Kummerow, C., and L. Giglio, 1994: A passive microwave technique for estimating rainfall and vertical structure information from space. Part II: Applications to SSM/I data. *J. Appl. Meteor.,* **33,** 19–34.

——, and Coauthors, 2000: The status of the Tropical Rainfall Measuring Mission (TRMM) after two years in orbit. *J. Appl. Meteor.,* **39,** 1965–1982.

——, and Coauthors, 2001: The evolution of the Goddard profiling algorithm (GPROF) for rainfall estimation from passive microwave sensors. *J. Appl. Meteor.,* **40,** 1801–1820.

Kuo, H.-L., 1965: On formation and intensification of tropical cyclones through latent heat release by cumulus convection. *J. Atmos. Sci.,* **22,** 40–63.

——, 1974: Further studies of the parameterization of the influence of cumulus convection on large-scale flow. *J. Atmos. Sci.,* **31,** 1232–1240.

Levit, N. L., K. K. Droegemeier, and F. Kong, 2004: High-resolution storm-scale ensemble forecasts of the March 28, 2000 Fort Worth tornadic storms. Preprints, *20th Conf. on Weather Analysis and Forecasting/16th Conf. on Numerical Weather Prediction,* Seattle, WA, Amer. Meteor. Soc*.,* CD-ROM, 23.6.

Lin, Y.-L., R. D. Farley, and H. D. Orville, 1983: Bulk parameterization of the snow field in a cloud model. *J. Climate Appl. Meteor.,* **22,** 1065–1092.

McCollum, J. R., A. Gruber, and M. B. Ba, 2000: Discrepancy between gauges and satellite estimates of rainfall in equatorial Africa. *J. Appl. Meteor.,* **39,** 666–679.

McCumber, M., W.-K. Tao, J. Simpson, R. Penc, and S.-T. Soong, 1991: Comparison of ice-phase microphysical parameterization schemes using numerical sumulations of tropical convection. *J. Appl. Meteor.,* **30,** 985–1004.

Meyers, M. P., P. J. DeMott, and W. R. Cotton, 1992: New primary ice-nucleation parameterizations in an explicit cloud model. *J. Appl. Meteor.,* **31,** 708–721.

Rutledge, S. A., and P. V. Hobbs, 1984: The mesoscale and microscale structure and organization of clouds and precipitation in midlatitude cyclones. XII: A diagnostic modeling study of precipitation development in narrow cold-frontal rainbands. *J. Atmos. Sci.,* **41,** 2949–2972.

——, E. R. Williams, and T. D. Keenan, 1992: The down under Doppler and electricity experiment (DUNDEE): Overview and preliminary results. *Bull. Amer. Meteor. Soc.,* **73,** 3–16.

Shin, D.-B., and C. Kummerow, 2003: Parametric rainfall retrieval algorithms of passive microwave radiometers. *J. Appl. Meteor.,* **42,** 1480–1496.

Short, D. A., and K. Nakamura, 2000: TRMM radar observations of shallow precipitation of the tropical oceans. *J. Climate,* **13,** 4107–4124.

Silva Dias, M. A. F., and Coauthors, 2002: A case study of convective organization into precipitating lines in the Southwest Amazon during the WETAMC and TRMM-LBA. *J. Geophys. Res.*, **107,** 8078, doi:10.1029/2001JD000375.

Smith, P. L., Jr., C. G. Myers, and H. D. Orville, 1975: Radar reflectivity factor calculations in numerical cloud models using bulk parameterization of precipitation. *J. Appl. Meteor.,* **14,** 1156–1165.

Steiner, M., R. A. Houze Jr., and S. E. Yuter, 1995: Climatological characterization of three-dimensional storm structure from operational radar and rain gauge data. *J. Appl. Meteor.,* **34,** 1978–2007.

Tao, W. K., and J. Simpson, 1993: Goddard cumulus ensemble model. Part I: Model description. *Terr. Atmos. Oceanic Sci.,* **4,** 35–72.

Wilheit, T. T., 1986: Some comments on passive microwave measurement of rain. *Bull. Amer. Meteor. Soc.,* **67,** 1226–1232.

——, A. T. C. Chang, M. S. V. Rao, E. B. Rodgers, and J. S. Theon, 1977: A satellite technique for quantitatively mapping rain rates over the oceans. *J. Appl. Meteor.,* **16,** 551–560.

Williams, E. R., S. A. Rutledge, S. G. Geotis, N. Renno, E. Rasmussen, and T. Rickenbach, 1992: A radar and electrical study of tropical "hot towers." *J. Atmos. Sci.,* **49,** 1386–1395.

Xue, M., K. K. Droegemeier, V. Wong, A. Shapiro, and K. Brewster, 1995: ARPS 4.0 user's guide. Center for Advanced Prediction Systems, The University of Oklahoma, 380 pp. [Available online at http://caps.ou.edu/ARPS/ARPS4.guide.html.]

——, ——, and ——, 2000: The Advanced Regional Prediction System (ARPS)—A multi-scale nonhydrostatic atmospheric simulation and prediction model. Part I: Model dynamics and verification. *Meteor. Atmos. Phys.,* **75,** 161–193.

——, and Coauthors, 2001: The Advanced Regional Prediction System (ARPS)—A multi-scale nonhydrostatic atmospheric simulation and prediction tool. Part II: Model physics and applications. *Meteor. Atmos. Phys.,* **76,** 143–165.

——, D. H. Wang, J. D. Gao, K. Brewster, and K. K. Droegemeier, 2003: The Advanced Regional Prediction System (ARPS), storm-scale numerical weather prediction and data assimilation. *Meteor. Atmos. Phys.,* **82,** 139–170.

Yuter, S. E., and R. A. Houze Jr., 1995: Three-dimensional kinematic and microphysical evolution of Florida cumulonimbus. Part II: Frequency distributions of vertical velocity, reflectivity, and differential reflectivity. *Mon. Wea. Rev.,* **123,** 1941–1963.

Zepeda-Arće, J., E. Foufoula-Georgiou, and K. K. Droegemeier, 2000: Space-time rainfall organization and its role in validating quantitative precipitation forecasts. *J. Geophys. Res.,* **105,** 10 129–10 146.

Ziegler, C. L., P. S. Ray, and N. C. Knight, 1983: Hail growth in an Oklahoma multicell storm. *J. Atmos. Sci.,* **40,** 1768–1791.

Zipser, E. J., and K. R. Lutz, 1994: The vertical profile of radar reflectivity of convective cells: A strong indicator of storm intensity and lightning probability? *Mon. Wea. Rev.,* **122,** 1951–1959.